A&A 415, 1113–1121 (2004)
DOI: 10.1051/0004-6361:20034416

Astronomy & Astrophysics

X-ray spectroscopy of the W UMa-type binary VW Cephei

P. Gondoin⋆

Space Science Department, European Space Agency – Postbus 299, 2200 AG Noordwijk, The Netherlands

Received 29 September 2003 / Accepted 31 October 2003

Abstract. VW Cephei, a W UMa-type binary system, was observed twice with a four week interval in October 2002 by the *XMM-Newton* space observatory. During the first observation, the source appears to be quiescent. A shallow dip in the X-ray light curve during primary eclipse indicates that the primary and secondary stars both contribute to the X-ray emission which could arise from an extended corona encompassing the two companions. Spectral fitting of the EPIC spectra suggests a corona configuration with little contribution from quiet regions, similar to the Sun. On the contrary, the 0.2–0.8 keV temperature of the "cool" plasma components is reminiscent of solar- type active regions, while the hot ($T \geq 1$ keV) component may be caused by disruptions of magnetic fields associated with flaring activity. During the second observation, a large flare occured in the corona above the primary component around the time of primary eclipse. The VW Cep count rate decayed by 30% in about 3.7 ksec and the emission measure of hot ($T > 10^7$ K) plasma varied by a factor of 4. The flare was comparable in size to two-ribbon flares observed on the Sun. Intense flaring activity on VW Cep is supported by a neon abundance enhancement relative to oxygen reminiscent of abundance anomalies observed during solar and stellar flares. Compared with other active binary systems such as RS CVn or BY Dra, VW Cep has relatively less material at temperatures higher than 10^7 K and the temperatures of hot plasmas appear to be lower.

Key words. stars: individual: VW Cephi – stars: activity – stars: coronae – stars: evolution – stars: late-type – X-rays: stars

1. Introduction

VW Cephei (HD 197433 = BD+75°752; $V = 7.38$) is a close binary system ($\pi = 0.041''$; ESA 1997) with an extremely fast rotation and revolution period of only 6^h41^m. It is a well-known representative of the W UMa stellar class which consists of eclipsing binaries with late F–K spectral type components in contact via a common convective envelope. Strong tidal forces cause them to rotate synchronously. VW Cep (HD 197433), one of the most intensively studied W UMa system, is a partial eclipsing contact binary with components of spectral type KO V and G5V (Hill 1989). Using the Doppler imaging technique, Hendry & Mochnacki (2000) reported a very high spot coverage on both stellar components. A variable Hα emission from the secondary cooler component has been found to be correlated with the presence of photospheric spots (Frasca et al. 1996). Radio observations of VW Cep shows that a very weak source may be associated with the quiescent coronal emission (Rucinski & Seaquist 1988). A comparison of the relative line fluxes for selected strongest chromospheric, transition region, and low corona emission lines in VW Cep and a single rapidly rotating reference star showed that *Extreme Ultraviolet Explorer* data obtained in 1995 were consistent with period-independent saturated levels of activity for features forming at $T \leq 10^5$ K (Rucinski 1996). Observational data also indicate a variable chromospheric and coronal activity on VW Cephi, both regular and of a flaring nature (Bradstreet & Guinan 1990; Pustylnik 1995; Hendry & Mochnacki 2000).

W UMa type stars are strong X-ray emitters but with luminosities lower, in general, than those of the detached, subgiant RS CVn type binaries, possibly due to saturation effects (Vilhu & Heise 1986; Stepien et al. 2001). Since the components in W UMa systems have the shortest periods possible for two non-degenerate main-sequence stars, these objects are of great interest in the study of the relation between stellar rotation rate and X-ray activity. VW Cep was the first contact binary detected in X-rays with *HEAO1* (Caroll et al. 1980). It was later observed with the Imaging Proportional Counter (IPC) and with the Solid State Spectrometer on board *Einstein* (Cruddace & Dupree 1984). Using *EXOSAT*, Vilhu & Heise (1990) reported evidence of phase dependant X-ray emission from VW Cep. Further *EXOSAT* observations (Vilhu et al. 1988) did not reveal any orbital modulation, although VW Cep did show a large flare. A day-long *Ginga* observation (Tsuru et al. 1992) of VW Cep revealed no flaring or orbital modulation but suggested the presence of persistent hot gas with a temperature of about 10^6 K. An X-ray flare on VW Cep was detected by McGale et al. (1996) in a *ROSAT* PSPC survey of W UMa systems, where the flux increased by a factor of two relative to the quiescent flux level, the temperature of the hot plasma increased by a factor of about 1.5 and its emission measure rose by a factor of almost 5. Using *ASCA* data, Choi & Dotani (1998) found a long duration flare that they interpreted in terms of a two-ribbon flare model. A significant dip in the X-ray flare

⋆ e-mail: pgondoin@rssd.esa.int

Table 1. VW Cephei observation log during revolutions 515 and 529.

Rev.	Experiment	Filter	Mode	Start Exp.(UT)	Exp. Duration
515	MOS1	Thick	Full frame	2002-10-02@08:53:54	17 245 s
	MOS2	Thick	Full frame	2002-10-02@08:53:53	17 255 s
	p−n	Thick	Full frame	2002-10-02@09:15:56	15 959 s
	RGS1		Spec + Q	2002-10-02@08:53:10	16 870 s
	RGS2		Spec + Q	2002-10-02@08:52:20	17 221 s
529	MOS1	Thick	Full frame	2002-10-30@05:58:37	11 669 s
	MOS2	Thick	Full frame	2002-10-30@05:58:34	11 673 s
	p−n	Thick	Full frame	2002-10-30@06:20:38	10 048 s
	RGS1		Spec + Q	2002-10-30@05:57:52	11 911 s
	RGS2		Spec + Q	2002-10-30@05:57:52	11 915 s
	OM	*U*	Image	2002-10-30@06:03:48	4000 s
	OM	*UVW1*	Image	2002-10-30@07:37:16	4100 s

curve, also detected earlier by Vilhu et al. (1988) was identified as an eclipse by the secondary star.

We provide analysis results of X-ray spectra of VW Cephei registered during two observations performed in October 2002 with the *XMM-Newton* observatory. The paper is organized as follows. Section 2 describes the X-ray observations of VW Cep and the data reduction procedures. Section 3 presents the integrated flux measurements and their temporal behavior during the observations. Sections 4 and 5 describe the spectral analysis of the EPIC and RGS data sets. Finally, an interpretation of the analysis results is given in Sect. 6.

2. Observations and data reduction

VW Cephei was observed twice by the *XMM-Newton* space observatory (Jansen et al. 2001), respectively in revolution 515 on 2002 October 2 and in revolution 529 on 2002 October 30 (see Table 1). The satellite observatory uses three grazing incidence telescopes which provide an effective area higher than 4000 cm^2 at 2 keV and 1600 cm^2 at 8 keV (Gondoin et al. 2000). Three CCD EPIC cameras (Strüder et al. 2001; Turner et al. 2001) at the prime focus of the telescopes provide imaging in a 30 arcmin field of view and broadband spectroscopy with a resolving power of between 10 and 60 in the energy band 0.3 to 10 keV. Two identical RGS reflection grating spectrometers behind two of the three X-ray telescopes allow higher resolution ($E/\Delta E$ = 100 to 500) measurements in the soft X-ray range (6 to 38 Å or 0.3 to 2.1 keV) with a maximum effective area of about 140 cm^2 at 15 Å (den Herder et al. 2001). VW Cephei observations were conducted with the EPIC cameras operating in full frame mode (Ehle et al. 2001). RGS spectra were recorded simultaneously. During revolution 529, short optical/UV observations were also performed with the 30 cm Optical Monitor (OM) aboard *XMM-Newton* (Mason et al. 2001) using the *U* and *UVM1* filters. "Thick" aluminum filters were used in front of all EPIC cameras to reject visible light from the star itself. Processing of the raw event dataset was performed using the "emchain", "epchain" and "rgsproc" pipeline tasks of the *XMM-Newton* Science Analysis System (SAS version 5.3.0). VW Cep spectra were built from photons detected within a window of about 50″ diameter around the target boresight. The background was estimated on the same CCD chips as the source, within windows of similar sizes which were offset from the source position in an empty field region. The SAS task "epatplot" was used to verify that the count rate of the target does not produce pile-up effect in the core of the telescope point spread function registered by the EPIC cameras. The Pulse-Invariant (PI) spectra were rebinned such that each resulting MOS channel had at least 20 counts per bin and each p−n channel had at least 40 counts per bin. χ^2 minimization was used for spectral fitting. All fits were performed using the XSPEC package (Arnaud & Dorman 2001). The EPIC and RGS response matrices were generated by the SAS task "rmfgen" and "rgsrmfgen" respectively. EPIC p−n, MOS 1 and MOS 2 spectra were fitted together. The RGS spectra were analyzed separately due to their higher spectral resolution in the 0.3−2.1 keV energy range.

3. Integrated flux and temporal behaviour

Figure 1 shows the light curves of VW Cephei obtained with the p−n camera during revolutions 515 and 529. In each graph, the upper curve is the count rate in the 0.3 to 2 keV band and the lower curve is the count rate above 2 keV. The count rates are on average comparable in both revolutions but the light curves show different behaviors. During revolution 515, the count rate is approximately constant at a rate of about 2.3 s^{-1} with a 20% drop of 2.3 ksec duration in the middle of the observation. This count rate variation is reminiscent of a dip found by Choi & Dotani (1998) in the X-ray curves and also detected earlier by Vilhu et al. (1988). The dip occurs around JD = 2 452 549.98 which corresponds to orbital phases in the range $0.055 < \phi < 0.156$ according to the ephemeris given in Kaszas et al. (1998). Hence, this dip could be the result of an eclipse since its phase is close to the primary eclipse expected from the optical data. The primary, i.e. the deepest eclipse of VW Cep which by definition corresponds to phase 0.0 occurs when the secondary star (M = 0.25 $M_\odot$, R = 0.5 $R_\odot$) is occulted by its larger companion (M = 0.9 $M_\odot$, R = 0.93 $R_\odot$). The presence of a dip in the X-ray light curve during the primary eclipse indicates that the secondary star also contributes

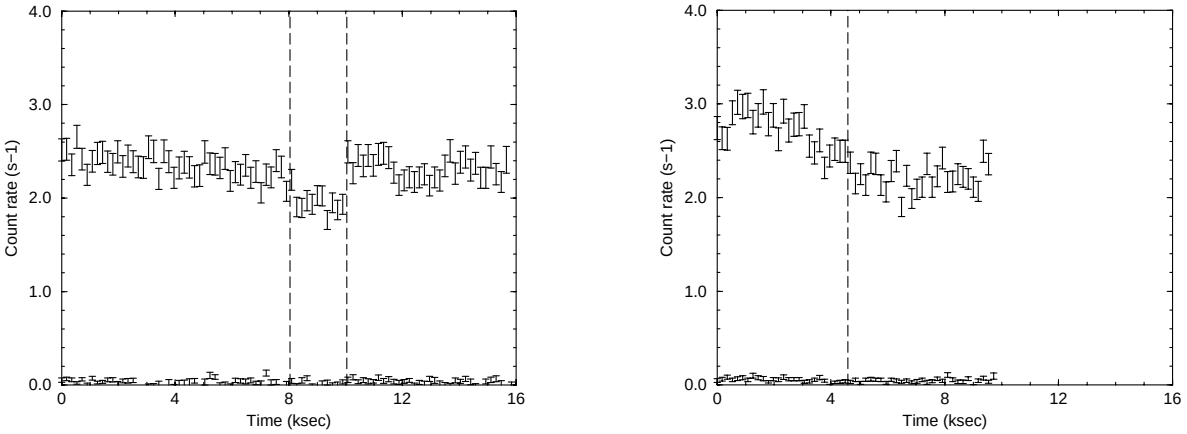

Fig. 1. Light curves of VW Cephei obtained with the EPIC p−n camera during revolution 515 between orbital phases 0.72 and 0.39 (left) and during revolution 529 between orbital phases 0.89 and 0.31 (right). In each graph, the upper curve is the count rate in the 0.3 to 2 keV band and the lower curve is the count rate in the 2 to 10 keV band. The events are binned in 180 s time intervals. The two vertical dashed lines in the left graph indicate the count rate dip period between orbital phases 0.06 and 0.16. The single vertical dashed line in the right graph separates the high flux period ($\phi < 0.08$) from the low steady flux period ($\phi > 0.08$).

to the X-ray emission. The observation performed during revolution 515 covers the orbital phases 0.72 to 0.39 but does not include the time of secondary eclipse which could induce a second dip in the X-ray light curve.

The observation performed during revolution 529 also covers a range of orbital phases (ϕ = 0.89 to 0.31) around the primary eclipse. Its light curve (see Fig. 1) starts with a high count rate which keeps rising for about 1 ksec and then decreases by about 30% during the next 4 ksec. During the second half of the exposure, the count rate remains approximately constant at about 2.2 s^{-1}. Contrary to the observation of revolution 515, no dip is observed in the light curve around the primary eclipse which occurs 2.5−2.9 ksec after the start of the observation. This suggests that, during revolution 529, most of the X-ray emission was coming from the larger, more massive companion.

The spectral analysis of each observation was conducted separately for two flux levels. The spectral analysis of revolution 515 and 529 data was performed in two time intervals when count rates were respectively lower and higher than 2.6 cts s^{-1} in the 300 eV to 10 keV band of the p−n cameras. In revolution 515, these intervals correspond to the short 2.5 ksec dip in count rate in the middle of the observation and to the steady flux period at the beginning and at the end of the observation. In revolution 529, these intervals correspond to the high flux level of about 4 ksec at the beginning of the exposure and to the steady low flux level observed during the remaining part of the observation. Spectral fitting of EPIC data (see Sect. 4) during these four periods yields flux measurements in the 0.3−2 keV and 2−4 keV bands. These measurements were converted into X-ray luminosities $L_{0.3-2\ \mathrm{keV}}$ and $L_{>2\ \mathrm{keV}}$ using *Hipparcos* parallax data (ESA 1997). Results are given in Table 2 including hardness ratios *hr* of the X-ray emission defined as $hr = (L_{>2\mathrm{keV}} - L_{0.3-2\ \mathrm{keV}})/(L_{>2\ \mathrm{keV}} + L_{0.3-2\ \mathrm{keV}})$. The X-ray spectrum of VW Cephi is soft during both revolutions. The X-ray luminosity is more than 10 times higher in the 0.3−2 keV band than in the 2−4 keV band and no significant signal is detected above 4 keV. Table 2 indicates that the dip in the revolution 515 count rate corresponds to a luminosity drop of about 8% and that the X-ray luminosity varied by 20% during revolution 529.

Table 2. X-ray luminosities of VW Cephei in the 0.3−2 keV and 2−4 keV energy bands averaged over the different observations periods and corrected for interstellar absorption. The percentage contribution in flux of hot plasmas ($kT \geq 1$ keV) is indicated between bracketts.

Obs.	$L_{0.3-2\ \mathrm{keV}}$ (10^{28} erg s^{-1})	$L_{>2\ \mathrm{keV}}$ (10^{28} erg s^{-1})	*hr*
Rev. 515	52.5	3.1	–0.89
(steady cr)	(18%)	(61%)	
Rev. 515	48.1	2.4	–0.90
(dip)	(31%)	(75%)	
Rev. 529	63.8	3.0	–0.91
(high cr)	(31%)	(70%)	
Rev. 529	43.8	2.5	–0.89
(low cr)	(9%)	(45%)	

4. Spectral analysis of EPIC data

The four EPIC datasets (see Fig. 2) were fitted separately with the MEKAL optically thin plasma emission model (Mewe et al. 1985). The spectral fitting was performed in the 0.3–3 keV spectral bands for both revolutions. The interstellar hydrogen column density was left free to vary. N_{H} values in the range (2.7–6.4) $\times$ 10^{20} cm^{-2} were derived from the analysis of the two datasets which are lower than the total galactic H I column density $N_{\mathrm{H}} = 11.4 \times 10^{20}$ cm^{-2} (Dickey & Lockman 1990) in the direction of VW Cep. No single temperature plasma model that assumes either solar photospheric (Anders & Grevesse 1989) or non-solar abundances can fit the data, as unacceptably large values of χ^2 were obtained. The MEKAL plasma models with two components at different temperatures prove barely

Table 3. Best fit parameters to EPIC data using a 3 components MEKAL model (Mewe et al. 1985). The spectral fitting was conducted in the 0.3–4 keV band with the same abundance relative to the Sun for all components.

	Revolution (Steady cr)	515 (dip)	Revolution (high cr)	529 (low cr)
$N_{\rm H}$ (10^{20} cm^{-2})	2.1 ± 0.5	3.4 ± 1.1	4.5 ± 0.7	1.4 ± 0.9
Z	0.24 ± 0.02	0.22 ± 0.03	0.20 ± 0.02	0.23 ± 0.03
kT_1 (keV)	0.35 ± 0.01	0.31 ± 0.06	0.27 ± 0.02	0.39 ± 0.02
EM_1 (10^{52} cm^{-3})	2.3 ± 0.4	1.6 ± 1.3	2.5 ± 0.7	2.2 ± 0.6
kT_2 (keV)	0.72 ± 0.02	0.60 ± 0.06	0.62 ± 0.03	0.78 ± 0.02
EM_2 (10^{52} cm^{-3})	2.9 ± 0.3	2.6 ± 0.9	3.8 ± 0.5	2.7 ± 0.5
kT_3 (keV)	1.36 ± 0.06	1.05 ± 0.08	0.99 ± 0.05	1.8 ± 0.3
EM_3 (10^{52} cm^{-3})	1.3 ± 0.2	1.9 ± 0.6	2.6 ± 0.6	0.6 ± 0.3
χ^2	1.43 (876/611 d.o.f.)	1.07 (406/378 d.o.f.)	1.17 (583/498 d.o.f.)	1.19 (532/446 d.o.f.)

acceptable. Hence, the EPIC spectra of VW Cep were fitted using a MEKAL model with three components at different temperatures but having the same metallicity. The improvement in χ^2 statistics with respect to the two temperature model is significant to a >99% confidence level using the F-statistic. The addition of a fourth component to the model does not further improve the quality of the spectral fit.

The temperatures of the coolest plasma components at $T \approx 4 \times 10^6$ K and 8×10^6 K are similar in revolution 515 and 529. The temperature of the hottest plasma component varies in the range (1–2) $\times 10^7$ between the different analysis periods. The average element abundance in the VW Cep corona is found to be lower than the solar photospheric value (see Table 3) and no significant abundance variation is detected. The three component model suggests that 70% or more of the emission measure is provided by plasmas with temperatures in the range (3−9) $\times 10^6$ K. These are the main source of X-ray emission in the soft energy band below 2 keV. Hot ($T > 10^7$ K) plasmas in VW Cep have a lower emission measure. They are the main sources of X-ray emission in the hard X-ray band above 2 keV during revolution 515 and during the high count period of revolution 529. They contribute to less than 50% of the X-ray luminosity above 2 keV during the low count rate period of revolution 529. Among all of the different changes, eruption and instabilities seen on the Sun, the ones labeled "flares" all have in common material heated to temperatures of 10^7 K or higher (Golub & Pasachoff 1997; Reale et al. 2001). Such temperatures are not seen in the non-flaring corona, and events that do not produce such hot plasmas are not called flares. It has also been proposed that the peak in emission measure around 10^7 K of active stellar coronae is due to flaring activity (Drake et al. 2000; Sanz-Forcada et al. 2002). Such flaring activity is expected to induce count rate fluctuations as observed in the EPIC light curves of VW Cephi during revolution 529. Thus, the existence of significant amounts of $>10^7$ K material and the 30% count rate decay over 3.7 ksec during revolution 529 are indicative of a flare. The occurrence of a large flare during revolution 529 is corroborated by the large decay in the emission measure of hot plasmas between the high and low count rate periods of revolution 529 (see Table 3). This flare probably occurred in the corona of the primary companion since the decay was observed at the time of the primary eclipse when the secondary star is occulted and no dip was observed in the light curve.

5. Spectral analysis of RGS data

Because of the lower effective area and larger spectral resolution of the RGS experiment compared with the EPIC camera, we did not divide the RGS exposures in periods corresponding to low and high count rates. Instead, we compared the RGS spectrum averaged over revolution 529 with the one averaged over revolution 515. This approach provides higher signal to noise ratio spectra at the expense of time resolution. EPIC analysis results will be kept in mind which indicate that the X-ray emission was relatively constant during revolution 515 but was significantly variable during revolution 529. The RGS 2 datasets only could be used for analysis. The RGS 2 spectra of VW Cephi were fitted with a VMEKAL model with two components at different temperatures. The VMEKAL model generates a spectrum of hot diffuse gas with line emission from several elements based on the calculation of Mewe et al. (1985) with Fe L calculations by Liedahl (1995). Hence, two electron temperatures and electron densities are assumed for the entire ensemble of element charge states and in particular for iron, oxygen and neon which produce the most prominent lines. This assumption turns out to be fairly adequate within the observational uncertainties of the present spectra (see Fig. 3). The model temperatures of the plasma components and their average abundance were left free to vary. The abundances of the O and Ne elements which give prominent lines in the considered spectral range were allowed to vary independently but with the same value for the two temperatures components. The best fit parameters are given in Table 4. The temperatures and the emission measures of the plasma components are similar to the values of the low and mid-temperature components derived from the analysis of EPIC spectra with a three component model (see Table 3). In revolution 515, the oxygen and neon abundance are respectively a factor of about 3 and 4 higher than the average abundance of the other elements. In revolution 529, the oxygen abundance is similar to the abundance of the other elements and the neon abundance is a factor of two higher. Time averaging of the RGS spectrum during

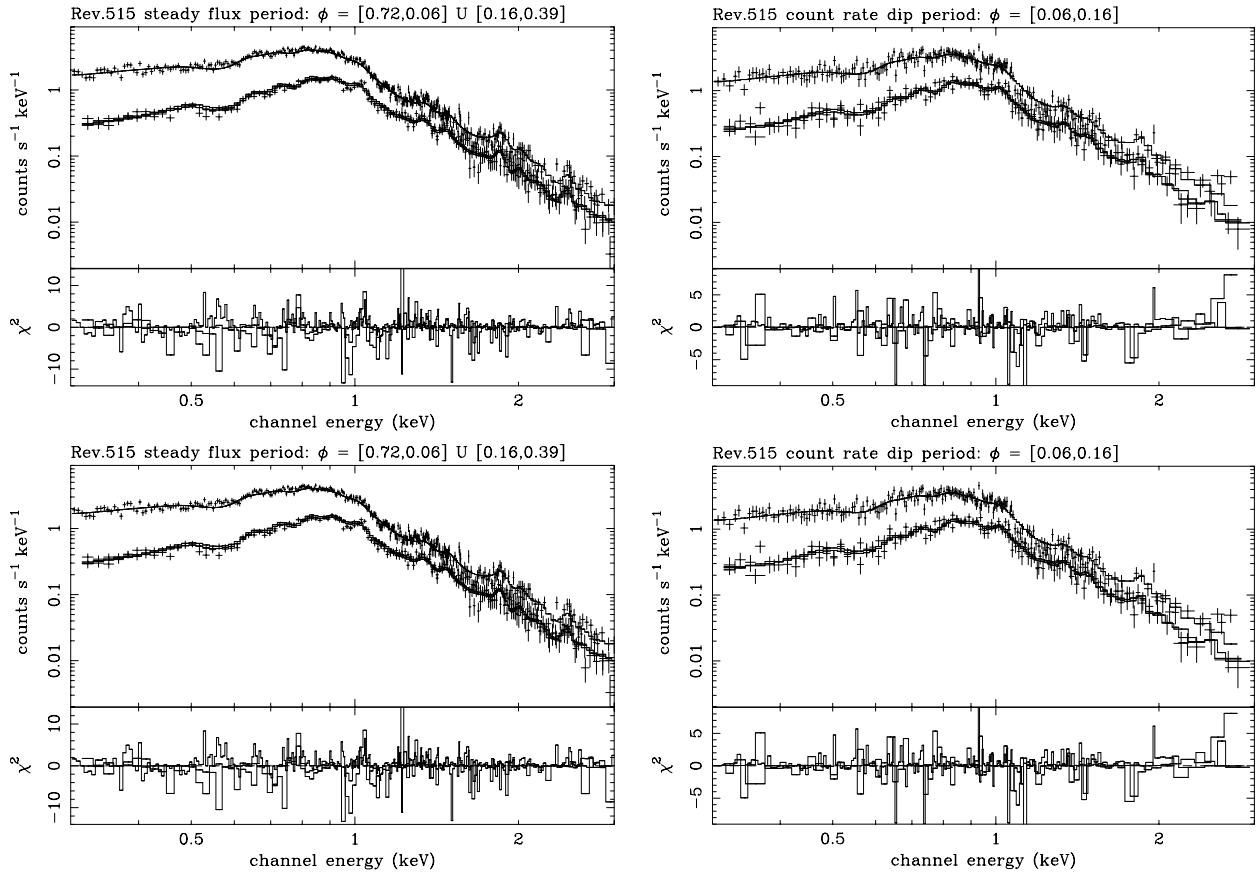

Fig. 2. *Top*: best fit model to EPIC revolution 515 spectra during the steady flux period (left) and during the short count rate dip period (right). *Bottom*: best fit model to revolution 529 spectra during the high flux period (left) and during the low steady flux (right). The EPIC data (crosses) and spectral fit (solid line) are shown in the upper panel and the χ^2 contributions in the lower panel of each graph.

Table 4. Best fit parameters derived from RGS 2 spectra using a VMEKAL model with two temperature components.

	Revolution 515	Revolution 529
$N_{\rm H}$ (10^{20} cm^{-2})	4.4 ± 0.3	2.3 ± 0.2
kT_1 (keV)	0.35 ± 0.05	0.20 ± 0.02
EM_1 (10^{52} cm^{-3})	1.1 ± 0.5	4.0 ± 2.6
kT_2 (keV)	0.56 ± 0.03	0.66 ± 0.02
EM_2 (10^{52} cm^{-3})	2.3 ± 0.5	5.0 ± 1.0
O	0.27 ± 0.06	0.06 ± 0.02
Ne	0.37 ± 0.15	0.15 ± 0.05
Other abundances	0.10 ± 0.01	0.08 ± 0.02
χ^2	1.28 (183/143 d.o.f.)	1.18 (378/321 d.o.f.)

revolution 529 prevents any direct comparison of the element abundances between the quiescent and flare X-ray levels. The determination of abundances relative to hydrogen requires an accurate measurement of the X-ray continuum which cannot be reliably measured even from the RGS spectra due to their moderate spectral resolution and signal to noise ratio (see Fig. 3). Therefore it is modeled from the flux left over when all of the known emission lines in the VMEKAL model are included. No plasma spectroscopy code includes all of the emission lines, so the missing weak emission lines are misinterpreted as continuum flux (Schmitt et al. 1996), thereby raising the hydrogen abundance derived from the free-free continuum and lowering all of the metal abundances relative to hydrogen. This systematic error in the metal abundances relative to hydrogen is not included in the abundance uncertainties stated in Table 4 but the fitting results suggest that the neon abundance is significantly higher than the abundance of the other elements. In particular, the Ne/O ratio found for VW Cep seems to be higher than in the solar photosphere. The indication of a Ne abundance enhancement is reminiscent of a similar anomaly observed in a subset of solar flares (Murphy et al. 1991; Schmelz 1993). Large Ne abundance enhancements are a common feature of active stellar coronae (Güdel et al. 2001a,b; Huenemoerder et al. 2001) and an inverse FIP effect is observed in very active coronae (Brinkman et al. 2001; Drake et al. 2001) where the abundances (relative to oxygen) increase with increasing first ionization potential (FIP).

Figure 3 shows the RGS 2 spectra of VW Cephi averaged over revolution 515 and 529. Line fluxes and positions were measured using the XSPEC package by fitting the RGS spectra with a sum of narrow Gaussian emission lines convolved with the response matrice of the instrument. The continuum emission was described using bremstrahlung models with temperatures frozen to the best fit values derived by spectral fitting (see Table 4). All the strong lines were included in the fit. For line identification, we required only that the wavelength coincidence be comparable to the spectral resolution of

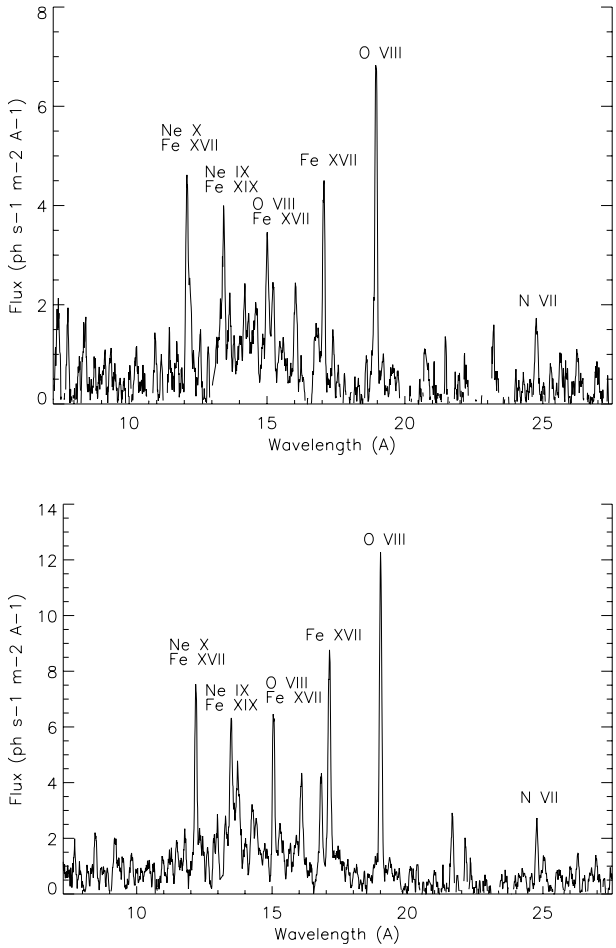

Fig. 3. Averaged first order spectra of RGS obtained during revolutions 515 (top) and 529 (bottom).

the RGS spectrometers, namely 0.04 Å over the 10 to 20 Å wavelength range. In the X-ray domain, several candidate lines may exist within this acceptable wavelength coincidence range. Hence, we only looked for resonance transitions of abundant elements and predicted line intensities using spectra of the Sun (Doschek & Cowan 1984) and of Capella (Brinkman et al. 2000). Series of lines of highly ionized Fe and several lines of the Ly and He series are visible in RGS spectra, most notably from O and Ne. Estimates of line fluxes are reported in Table 5. Their temperatures of maximum formation range between 3×10^6 K and 6×10^6 K suggesting that the corresponding ions are mainly associated with the cool plasma components inferred from EPIC data. However, lines such as the O VIII and Ne X lines have emissivity functions quite spread in temperature to which material present in the hot component contributes. No significant line intensity variations are observed between revolutions 515 and 529. The Ne X (12.13 Å), Ne IX (13.45 Å) and O VIII (16.01 Å) are affected by blends. This could explain why their fluxes (see Table 5) are inconsistently high compared with the values expected from the analysis of EPIC spectra.

6. Discussion

6.1. Structure of VW Cep corona

VW Cephei was observed twice at a four week interval in October 2002 by the *XMM-Newton* space observatory. In the first observation, the source appears to be quiescent with a shallow dip in the X-ray light curve during primary eclipse. In the second observation, the count rate first increased and then decayed to its quiescent level by about 30% in 3.7 ksec. The spectral fitting of the EPIC spectra of VW Cep at different periods with a three temperature component model suggests a corona configuration with little contribution from quiet regions, similar to the Sun. On the contrary the 0.2–0.8 keV temperature of the "cool" components is reminiscent of solar type active regions, while the hot ($T \geq 1$ keV) component may be caused by disruptions of magnetic fields associated with flaring activity. The review of coronal activity by Vaiana & Rosner (1978) pointed out that the Sun, if completely covered by active regions, would have an X-ray luminosity of 20×10^{28} ergs s^{-1}. When scaled to the surfaces of VW Cep components ($R_1 \approx 0.93\ R_\odot$ and $R_2 \approx 0.5\ R_\odot$; Pustylnik & Niarchos 2000), X-ray luminosities of 17×10^{28} erg s^{-1} and 5×10^{28} erg s^{-1} are obtained for the primary and secondary companions, respectively. These values are lower than the observed luminosity of VW Cep ($(46-56) \times 10^{28}$ erg s^{-1}) derived using *Hipparcos* parallaxes (see Table 2). They are also lower than the X-ray luminosity contribution ($\approx(33-45) \times 10^{28}$ erg s^{-1}) of the "cool" ($T < 1$ keV) plasma components. Following a simple rule of thumb, an extended corona encompassing the two companions ($d_{\rm sep} = 2.10 \pm 0.04\ R_\odot$; Hendry & Mochnacki 2000) is needed to explain the X-ray luminosity of the "cool" ($T < 1$ keV) plasmas with bright loops similar to those found in solar active regions. Such an extended corona could explain that only a shallow dip is observed in the X-ray light curves around the primary eclipse during revolution 515 (see Fig. 1). Assuming that these loop systems are static and each consists of similar loops of constant pressure p (dyn cm^{-2}), temperature T (K) and cross section, a characteristic loop length scale is obtained (Mewe et al. 1982) using the relation $T = 1400(pL)^{1/3}$ (Rosner et al. 1978):

$$L_{10} = 7.4 \times F \times T_7^4 \times EM_{52}^{-1} \times (R/R_\odot)^2 \quad (1)$$

where L_{10} is the loop half length in units of 10^{10} cm, T_7 is the coronal temperature in unit of 10^7 K, and EM_{52} is the emission measure in units of 10^{52} cm^{-3}. Inserting the observed temperature and emission measures (see Table 3) of the cold ($T < 1$ keV) components, characteristic loop sizes in the range $(0.8-3.4) \times 10^9$ cm and $(14-51) \times 10^9$ cm are obtained for temperatures of the two coolest plasma components in the ranges $T_1 = (3.4-4.5) \times 10^6$ K and $T_2 = (7.0-9.1) \times 10^6$ K, respectively. The RTV scaling law neglects gravity, assumes a constant cross-section, uniform heating, constant pressure and a monotonic increase of temperature with height. Since it turns out that the loop lengths derived using the RTV model are comparable with the pressure scale height H on each star, the assumption of constant pressure in the loops is barely justified. Furthermore, Schrijver et al. (1989) questioned the assumption

Table 5. Measured positions and flux estimate or upper limits of the strongest lines in the RGS spectra of VW Cephi obtained during revolutions 515 and 529. The columns give the predicted line positions, the measured line positions during revolution 515, the measured line positions during revolution 529, the ion and line identifications, the temperatures of maximum line formation, the line fluxes measured during revolution 515 and the line fluxes measured during revolution 529.

$\lambda_{\rm pred}$ (Å)	$\lambda_{\rm rev\ 515}$ (Å)	$\lambda_{\rm rev\ 529}$ (Å)	Ion	line ID	log ($T_{\rm m}$) log (K)	$F_{\rm rev\ 515}$ (10^{-6} cm^{-2} s^{-1})	$F_{\rm rev\ 529}$ (10^{-6} cm^{-2} s^{-1})
12.13	12.13	12.14	Ne X	H1AB	6.80	61 ± 27	55 ± 28
12.12			Fe XVII	4C	6.75		
13.45	13.45	13.45	Ne IX	He4w	6.60	64 ± 27	84 ± 31
13.46			Fe XIX		6.90		
13.50			Fe XIX		6.90		
15.01	15.01	15.01	Fe XVII	3C	6.75	83 ± 29	51 ± 29
16.01	16.01	16.02	O VIII	H2	6.60	44 ± 27	33 ± 27
16.07			Fe XVIII	F3	6.80		
17.05	17.05	17.06	Fe XVII	3G	6.70	64 ± 34	79 ± 36
17.10			Fe XVII	M2	6.70		
18.97	18.97	18.96	O VIII	H1AB	6.50	128 ± 50	109 ± 54

of constant loop cross section. Schrijver (1987) noticed that coronal condensation over solar bipolar regions has a projected area roughly an order of magnitude larger than the area of the underlying photospheric plage, suggesting the ratio Γ of the loop cross section at the apex to the cross section at the footpoint is approximately $\Gamma \approx 10$. Vesecky et al. (1979) made numerical calculations for loop with cross sections increasing with height in a way resembling a line dipole. They find that the scaling law is modified by the change in the loop cross section with height. Schrijver et al. (1989) note that their numerical results can be conveniently approximated by $T = 1400\ \Gamma^{-0.1} \times (pL)^{1/3}$. Using this modified law, one finds that the constant Γ enters Eq. (1) to the sixth power and could dramatically increase the loop half-length making it even further inconsistent with the constant pressure hypothesis. This rather suggests the presence of large loop systems on VW Cep that support the existence of an extended corona.

6.2. Flaring activity on VW Cep

In the second observation during revolution 529, the count rate decayed by 30% in about 3.7 ksec and then remained constant to a quiescent level (see Fig. 1). The emission measure of hot ($T > 10^7$ K) plasma at the beginning of the observation was greater by a factor of 4 compared to quiescence. This emission measure variation of hot plasma is suggestive of a flare. The absence of a dip in the light curve indicates that the flare likely occurred in the corona above the primary component around the time of primary eclipse (see Sect. 4). Flares have been previously reported on VW Cep (Vilhu et al. 1988; McGale et al. 1996; Choi & Dotani 1998; Hendry & Mochnacki 2000). Flaring activity on VW Cep is also supported by a Ne abundance enhancement relative to oxygen (see Table 4) reminiscent of abundance anomalies observed during stellar and solar flares. However, compared with other active binary systems such as RS CVn or BY Dra (Dempsey et al. 1993), VW Cep has relatively less material at temperatures higher than 10^7 K and the temperature of this hot plasma component appear to be lower. Different approaches have been proposed to estimate characteristic parameters and in particular the size of flaring regions. Analytic approaches (van den Oord & Mewe 1989; Pallavicini et al. 1990; Hawley et al. 1995) using only rise and decay time are adequate for the analysis of a large flare for which only light curves are available. However, they tend to overestimate the size of the flaring regions, in particular in the presence of significant heating during the decay (Favata & Schmitt 1999). As an extreme example, assuming that the event during revolution 529 is related to a single flare event, we estimated the maximum size of this flare by equating the measured decay time, the so-called e-folding time, to the radiative cooling time (Pallavicini et al. 1990), i.e. $\tau_{\rm rad} = 3kT/nP(T)$ where n is the density, T the coronal temperature, k the Boltzmann constant and $P(T)$ the radiative loss function for unit emission measure. $P(T) \approx 2 \times 10^{-23}$ erg cm^3 s^{-1} for temperatures in the range $(1\text{–}4) \times 10^7$ K (Mewe et al. 1985). We then derived an upper limit to the flare-emitting volume V from the measured emission measure $EM = n^2V$. EM was estimated from the emission measure difference of high temperature plasmas (see Table 3) between the flare period and the quiescent period of revolution 529. By further assuming a single loop model with an aspect ratio $\alpha = 0.1$, we found an upper limit to the loop length of about 7.8×10^{10} cm (see Table 6), i.e. comparable with the radius of the VW Cep primary star.

Covino et al. (2001) showed that the volumes and densities of stellar flares provided by the Pallavicini et al. (1990) approach are not dissimilar to those derived from the hydrodynamic decay-sustained heating model of Reale et al. (1997). These authors showed by simulation and verified with *Yokhoh* observations of solar flares that flares decay approximately along a straight line in the $\log EM^{1/2} - \log T$ diagram. They found a relation $f(\chi) = \tau_{\rm lc}/\tau_{\rm th}$ between the slope χ of the decay path and the ratio between the observed decay time $\tau_{\rm lc}$ and

Table 6. Physical parameters of VW Cep flare during revolution 529 compared with solar compact and two-ribbon flares (Pallavicini et al. 1990 and references therein).

	Solar compact flare	Solar 2-ribbon flare	VW Cep flare
L_X (erg s^{-1})	10^{26}–10^{27}	10^{27}–10^{28}	2×10^{30}
τ (s)	10^2–10^3	10^4	3.7×10^3
T (K)	(1–3) 10^7	(1–3) 10^7	1.2×10^7
EM (cm^{-3})	10^{48}–10^{49}	10^{49}–10^{50}	2×10^{52}
n (cm^{-3})	10^{11}–10^{12}	10^{10}–10^{11}	>6.5 10^{10}
V (cm^3)	10^{26}–10^{27}	10^{28}–10^{29}	$<5 \times 10^{32}$
L (cm)	(0.5–5) 10^9	10^{10}	$<8 \times 10^{10}$
B_{min} (G)	100–300	50–100	>60

the thermodynamic cooling time of the loop without additional heating τ_{th}. The loop length L is proportional to the characteristic decay time, but in the presence of significant heating during the decay, L is significantly reduced by a factor $f(\chi) > 1$, i.e. (Reale 2001):

$$L_9 = \tau_{lc}.T_7^{1/2}/120.f(\chi) \quad (2)$$

where L_9 and T_7 are in units of 10^9 cm and 10^7 K. When applied to the single flare event observed during revolution 529 (i.e. $\tau_{lc} = 3.7 \times 10^3$ s and $T = 1.2 \times 10^7$ K), a loop length $L = 3.2 \times 10^{10}/f(\chi)$ cm is obtained. Without high enough count rates for time resolved spectroscopy during revolution 529 flare, the slope χ of the locus of point in the $\log EM^{1/2} - \log T$ diagram cannot be estimated. Therefore, the correction factor $f(\chi)$ is unknown. In a large fraction of the solar flares examined by Reale et al. (1997) significant heating is present, so that the thermodynamic decay time of the loop alone overestimates its size by factors between 2 and 10. A factor $f(\chi)$ of 2 to 4 was found by Favata et al. (2000) in a systematic analysis of four large flares observed on the eclipsing binary Algol with *GINGA*, *EXOSAT*, *ROSAT* and *BeppoSAX*. Assuming similar long lasting heating during the decay phase of revolution 529 flare, loop lengths in the range $(6-16) \times 10^{10}$ cm are obtained which are comparable with the radius of VW Cep primary star. The X-ray flare on VW Cep would be comparable in size to the two-ribbon flares observed on the Sun (see Table 6). A flaring region of similar size has been detected in *ASCA* data by Choi & Dotani (1998) and was also interpreted by these authors in terms of a two-ribbon flare occurring on the primary star. Such evolving loop arcades are the result of different physical processes than the single, constant-volume loop which are assumed in the Reale et al. (1997) analysis. This would imply different physical conditions compared to the hydrodynamic simulation of Reale et al. (1997), and thus larger uncertainties on the interpretation of the transient event observed during revolution 529.

7. Summary

VW Cephei was observed twice with a four weeks interval in October 2002 by the *XMM-Newton* space observatory. In the first observation, the source appears to be quiescent with a shallow dip in the X-ray light curve during primary eclipse. Spectral fitting of VW Cep data suggests a corona configuration with little contribution from quiet regions, similar to the Sun. On the contrary the 0.2−0.8 keV temperature of the "cool" components is reminiscent of solar type active regions. An extended corona encompassing the two companions is needed to explain the X-ray luminosity of the "cool" ($T < 1$ keV) plasmas with bright loops similar to those found in solar active regions. Such an extended corona could explain why only a shallow dip is observed in the X-ray light curves around the primary eclipse during the first observation. The analysis also suggests the presence of large loop systems on VW Cep that supports the existence of an extended corona.

In the second observation, the count rate decayed by 30% in about 3.7 ksec and then remained constant to a quiescent level. The emission measure of hot ($T > 10^7$ K) plasma at the beginning of the observation was greater by a factor of 4 compared to quiescence. This emission measure variation of hot plasmas is suggestive of a flare. Flaring activity on VW Cep is also supported by a Ne abundance enhancement relative to oxygen reminiscent of abundance anomalies observed during stellar and solar flares. However, compared with other active binary systems such as RS CVn or BY Dra, VW Cep has relatively less material at temperatures higher than 10^7 K and the temperature of this hot plasma component appears to be lower. The absence of a dip in the light curve of the second observation indicates that the flare likely occurred in the corona above the primary component around the time of primary eclipse. Assuming that the event is related to a single flare event, loop lengths in the range $(6-16) \times 10^{10}$ cm are obtained which are comparable with the radius of VW Cep primary star. The X-ray flare on VW Cep would be comparable in size to the two-ribbon flares observed on the Sun.

Acknowledgements. I thank my colleagues from the *XMM-Newton* Science Operation Center for their support in implementing the observations. I am grateful to the anonymous referee for the helpful comments that allowed me to improve the paper.

References

Anders, E., & Grevesse, N. 1989, Geochim. Cosmochim. Acta, 53, 197

Arnaud, K., & Dorman, B. 2001, XSPEC User's Guide for version 11.1, `http://heasarc.gsfc.nasa.gov/docs/xanadu/xspec/manual/`

Bradstreet, D. H., & Guinan, E. F. 1990, in Active Close Binaries, ed. C. Ibanoglu (Dordrecht: Kluwer), 467

Brinkman, A. C., Gunsing, C. J. T., Kaastra, J. S., et al. 2000, ApJ, 530, 111

Brinkman, A. C., Behar, E., Güdel, M., et al. 2001, A&A, 365, L324

Carroll, R. W., Cruddace, R. G., Friedman, H., et al. 1980, ApJ, 235, L77

Choi, C. S., & Dotani, T. 1998, ApJ, 492, 761

Covino, S., Panzera, M. R., Tagliaferri, G., et al. 2001, A&A, 371, 973

Cruddace, R. G., & Dupree, A. K. 1984, ApJ, 277, 263

den Herder, J. W., Brinkman, A. C., Kahn, S. M., et al. 2001, A&A, 365, L7

Dempsey, R. C., Linsky, J. L., Schmitt, J. H. M. M., et al. 1993, ApJ, 413, 333
Dickey, J. M., & Lockman, F. J. 1990, ARA&A, 28, 215
Doschek, G. A., & Cowan, R. D. 1984, ApJS, 56, 67
Drake, J. J., Peres, G., Orlando, S., et al. 2000, ApJ, 545, 1074
Drake, N. A., Brickhouse, N. S., Kashyap, V., et al. 2001, ApJ, 548, L81
Ehle, M., Breitfellner, M., Dahlem, M., et al. 2001, The XMM−Newton Users' Handbook, http://xmm.vilspa.esa.es/user/AO2/uhb/xmm_uhb.html
ESA 1997, The Hipparcos Catalogue, ESA SP-1200
Favata, F., & Schmitt, J. H. M. M. 1999, A&A, 350, 900
Favata, F., Reale, F., Micela, G., et al. 2000, A&A, 353, 987
Frasca, A., Sanfilippo, D., & Catalano, S. 1996, A&A, 313, 532
Golub, L., & Pasachoff, J. M. 1997, in The Solar Corona, Cambridge UK, Cambridge University Press
Gondoin, P., Aschenbach, B., Erd, C., et al. 2000, SPIE Proc., 4140, 1
Güdel, M., Audard, M., Briggs, K., et al. 2001a, A&A, 365, L336
Güdel, M., Audard, M., Magee, H., et al. 2001b, A&A, 365, L344
Hawley, S. L., Fisher, G. H., Simon, T., et al. 1995, ApJ, 453, 464
Hendry, P. D., & Mochnacki, S. W. 2000, ApJ, 531, 467
Hill, G., Fisher, W. A., & Holmgren, D. 1989, A&A, 211, 81
Huenemoerder, D. P., Canizares, C. R., & Schulz, N. S. 2001, ApJ, 559, 1135
Jansen, F., Lumb, D., Altieri, B., et al. 2001, A&A, 365, L1
Kaszas, G., Vinko, J., Szatmary, K., et al. 1998, A&A, 331, 231
Liedahl, D. A., Osterheld, A. L., & Goldstein, W. H. 1995, ApJ, 438, 115
Mason, K. O., Breeveld, A., Much, R., et al. 2001, A&A, 365, L36
McGale, P. A., Pye, J. P., & Hodgkin, S. T. 1996, MNRAS, 280, 627
Mewe, R., Gronenschild, E. H. B. M., Heise, J., et al. 1982, ApJ, 260, 233
Mewe, R., Gronenschild, E. H. B., & van den Oord, G. H. J. 1985, A&A, 62, 197
Murphy, R. J., Ramaty, R., Reames, D. V., et al. 1991, ApJ, 371, 793
Pallavicini, R., Tagliaferri, G., & Stella, L. 1990, A&A, 228, 403
Pustylnik, I. B. 1995, ed. K. G. Strassmeier, Stellar Surface Structure, IAU Symo., 176, Wien, Poster Proc., 215
Pustylnik, I. B., & Niarchos, P. G. 2000, A&A, 361, 982
Reale, F., Betta, R., Peres, G., et al. 1997, A&A, 325, 782
Reale, F. 2001, in Stellar Coronae in the Chandra and XMM Era, ASP Conference Series, TBD, ed. F. Favata, & J. Drake
Reale, F., Peres, G., & Orlando, S. 2001, ApJ, 557, 906
Rosner, R., Tucker, W. H., & Vaiana, G. S. 1978, ApJ, 220, 643
Rucinski, S. M. 1998, AJ, 115, 303
Rucinski, S. M., & Seaquist, E. R. 1988, AJ, 95, 1837
SAS 2001, XMM-Newton Science Analysis System, Reference Documentation, http://xmm.vilspa.esa.es/user/sas_top.html
Sanz-Forcada, J., Brickhouse, N. S., & Dupree, A. K. 2002, ApJ, 570, 799
Schmelz, J. T. 1993, ApJ, 408, 373
Schmitt, J. H. M. M., Drake, J. J., & Stern, R. A. 1996, ApJ, 465, L51
Schrijver, C. J. 1987, A&A, 180, 241
Schrijver, C. J., Lemen, J. R., & Mewe, R. 1989, ApJ, 341, 484
Stepien, K., Schmitt, J. H. M. M., & Voges, W. 2001, A&A, 370, 157
Strüder, L., Briel, U., Dennerl, K., et al. 2001, A&A, 365, L18
Tsuru, T., Makishima, K., Ohashi, T., et al. 1992, MNRAS, 251, 221
Turner, M. J. L. T., Abbey, A., Arnaud, M., et al. 2001, A&A, 365, L27
Vaiana, G. S., & Rosner, R. 1978, ARA&A, 16, 393
van den Oordt, G. H. J., & Mewe, R. 1989, A&A, 213, 245
Vesecky, J. F., Antiochos, S. K., & Underwood, J. H. 1979, ApJ, 233, 987
Vilhu, O., & Heise, J. 1986, ApJ, 311, 937
Vilhu, O., Caillaut, J.-P., & Heise, J. 1988, ApJ, 330, 922